AMERICAN SOCIETY FOR MICROBIOLOGY | mBio

Check for updates

| Molecular and Cellular Biology | Research Article

Peptidoglycan DD-peptidases have distinct activities that impact fitness of *Acinetobacter baumannii*

Arshya F. Tehrani,[1] Abhisha Khadka,[1] Berenice Furlan,[1,2] Michael Whalen,[3] Jacob Biboy,[4] Orietta Massidda,[5] Waldemar Vollmer,[6] Joseph M. Boll[1]

AUTHOR AFFILIATIONS See affiliation list on p. 14.

ABSTRACT The gram-negative cell envelope is a critical interface between the bacterium and its environment, serving as a selective barrier for nutrient uptake and defense against harmful agents. It also facilitates environmental sensing and adaptive responses. Structurally, it comprises the outer membrane, inner membrane, and periplasmic space, which contains the peptidoglycan layer—a conserved polymer that maintains cell shape and withstands internal turgor pressure. Peptidoglycan consists of glycan strands connected by short peptides, forming a mesh-like structure. In gram-negative bacteria, most peptidoglycan subunits contain tetrapeptides, generated by DD-carboxypeptidases (DD-CPases) that cleave the terminal D-alanine from pentapeptides. Although gram-negative bacteria encode multiple DD-CPases, their precise roles in maintaining cell shape and structural integrity remain poorly understood. The nosocomial pathogen *Acinetobacter baumannii* encodes three putative DD-CPases. To investigate their functions, we generated single and double mutants in *dacC*, *dacD*, and *pbpG*, which encode homologs of *Escherichia coli* DD-CPases PBP5 and PBP6a, PBP6b, and the endopeptidase PBP7, respectively. We assessed the mutants for changes in cell morphology, growth dynamics, and pH-dependent stress tolerance. Additionally, we analyzed their peptidoglycan composition to determine the biochemical consequences of enzyme inactivation. Each mutant showed distinct alterations in coccobacillary morphology and growth. Peptidoglycan analysis showed DD-CPase activity, with PBP6b also exhibiting endopeptidase activity. Together, our results demonstrate that each peptidoglycan-modifying enzyme contributes uniquely to cell growth, morphology, and pH tolerance, underscoring their non-redundant functions.

IMPORTANCE DD-peptidases, including carboxypeptidases and endopeptidases, are crucial for maintaining cell envelope homeostasis, with distinct roles for each enzyme in cell wall biogenesis and structural integrity. The enzymatic characterization presented in this study not only advances our understanding of fundamental *Acinetobacter baumannii* biology but also highlights these enzymatic activities as targets for the development of innovative therapeutic strategies to combat infections caused by this multidrug-resistant microbe.

KEYWORDS DD-carboxypeptidase, peptidoglycan, outer membrane, gram-negative, cell envelope

The gram-negative cell envelope is structurally organized into three distinct layers, each critical for maintaining cellular integrity and environmental fitness. The hallmark of gram-negative bacteria is the asymmetric outer membrane (OM), which consists of an inner leaflet of glycerophospholipids and an outer (surface-exposed) leaflet enriched with lipopolysaccharide (LPS) or lipooligosaccharide. The lipid asymmetry forms a robust permeability barrier that restricts the entry of toxic compounds (1).

Editor Petra Anne Levin, Washington University in St. Louis, St. Louis, Missouri, USA

Address correspondence to Joseph M. Boll, Joseph.Boll@utdallas.edu.

The authors declare no conflict of interest.

See the funding table on p. 14.

Received 12 January 2026
Accepted 15 February 2026
Published 23 March 2026

Beneath the OM lies the cytoplasmic (inner) membrane, a symmetric bilayer composed of glycerophospholipids. Between the two membranes is the periplasmic space, which contains a thin peptidoglycan (PG) layer (2). The PG is the primary determinant of cell shape and mechanical strength, protecting the cell from osmotic lysis (3). However, recent studies suggest that the LPS-rich OM also contributes significantly to the mechanical stability and shape maintenance during osmotic changes (4, 5). Despite these insights, the molecular mechanisms that coordinate the biogenesis and integration of the OM and PG layers remain poorly understood. Emerging evidence points to direct interactions between PG maturation and the β-barrel assembly machinery (BAM) complex, suggesting a physical and functional linkage connecting the envelope layers (6). Disrupting these connections may represent a promising strategy to compromise envelope integrity and sensitize bacteria to environmental and antibiotic stress.

Penicillin-binding proteins (PBPs) are a diverse group of enzymes essential for the biosynthesis, maturation, and remodeling of the PG layer. These enzymes catalyze key reactions such as formation or breaking of peptide bonds, which are critical for forming and modifying peptide cross-links within the PG meshwork. PBPs are broadly categorized into high molecular weight (HMW) and low molecular weight (LMW) groups, each with distinct enzymatic functions that contribute to PG assembly and homeostasis (7). HMW PBPs are PG synthases and are further divided into two classes: Class A PBPs, which possess both glycosyltransferase and transpeptidase activities, and Class B PBPs, which function as transpeptidases (7, 8). The former enzymes are responsible for polymerizing glycan strands and cross-linking peptides, thereby constructing the PG scaffold. LMW PBPs are generally non-essential under standard growth conditions but play important roles in PG maturation, remodeling, and turnover (9–13). They function mainly as DD-endopeptidases (DD-EPases) and/or DD-carboxypeptidases (DD-CPases), cleaving amide bonds within stem peptides to regulate PG architecture and facilitate cell wall plasticity during growth and environmental adaptation (7, 14, 15).

DD-CPases are critical enzymes involved in the maturation and remodeling of the PG layer. These enzymes hydrolyze the peptide bond between the fourth and fifth amino acids (both usually D-Ala) of pentapeptides, thereby releasing a terminal D-alanine and generating tetrapeptides (16). This PG maturation occurs within minutes of the incorporation of new PG strands in *Escherichia coli* (17). Tetrapeptides, in turn, serve as substrates for various downstream cell envelope processes. In *Acinetobacter baumannii*, for instance, tetrapeptides are utilized by the LD-transpeptidase (LD-TPase) LdtJ to form alternative 3-3 crosslinks and add D-amino acids to position 4 of tetrapeptides in PG (18, 19). Beyond their role in PG architecture, tetrapeptides have been shown to bind to the BAM complex and inhibit the assembly of OM proteins, dampening OM protein assembly near mature PG (e.g., the old poles) during the cell cycle (6). Moreover, tetrapeptide formation has been implicated in establishing physical and functional connections between the PG layer and OM proteins, contributing to the overall stability of the cell envelope via LD-TPase-mediated attachment of the OM-anchored lipoprotein Lpp in *E. coli*. DD-CPases are broadly conserved across gram-negative bacteria (20), with orthologs identified in Enterobacterales, *Pseudomonas aeruginosa*, and *A. baumannii*.

E. coli encodes at least seven DD-CPases, including PBP4 (also has DD-EPase activity), PBP4b, PBP5, PBP6a, PBP6b, AmpC, and AmpH (21–25), as summarized in Table S1. In addition, class A PBPs can also have considerable DD-CPase activity (26). PBP5, encoded by *dacA*, is the most abundant DD-CPase in *E. coli* (27). Deletion of *dacA* along with at least two other DD-CPase genes results in minor morphological abnormalities, such as kinks, bends, or branches (28). However, significant morphological defects only arise when all DD-CPase genes are deleted, in addition to the deletion of *mrcA* (encoding PBP1A), highlighting their overlapping yet distinct functions in PG maintenance. When *E. coli* grows under low-pH conditions, PBP6b takes over as the most important DD-CPase from PBP5 (29). Under conditions of severe outer membrane biogenesis stress, the seemingly "minor" PBP6b, but not PBP5, becomes essential (30). The weak beta-lacta-

mase AmpC and the beta-lactamase AmpH also contribute to shape maintenance (25). Whether the other DD-CPases have specialized functions is not known.

In contrast, *A. baumannii* encodes only three predicted DD-CPase genes. *dacC* encodes a protein with high homology to both *E. coli* PBP5 (42% identity) and PBP6a (41% identity), denoted herein as PBP5/6a; *dacD* encodes PBP6b; and *pbpG* encodes PBP7, with the latter having both DD-EPase and DD-CPase activity (31), as summarized in Table S1. While *A. baumannii* PBP7 has both DD-EPase and DD-CPase activity (31), *E. coli* PBP7 has only DD-endopeptidase activity and has a role in cell division (32, 33). In *A. baumannii,* PBP7 has been shown to be important for bacterial survival during antibiotic treatment, although the precise mechanism underlying the increased susceptibility upon its inactivation remains unclear (31). The functional redundancy in *E. coli* contrasts with the streamlined DD-CPase system in *A. baumannii*, making it a powerful model for dissecting the specific contributions of individual DD-CPases to cell envelope integrity and bacterial fitness.

In this study, we generated targeted mutations in genes encoding the predicted DD-CPases, including *dacC* and *dacD*, and the predicted DD-CPase/DD-EPase *pbpG,* to investigate their individual and combined roles. We systematically assessed the morphological and physiological consequences of single and double mutations by analyzing changes in cell shape, growth kinetics, and sensitivity to environmental stress. Additionally, we analyzed the PG composition in the single mutants and biochemically defined the enzymatic activities of PBP5/6a and PBP6b. Our findings demonstrate that each DD-CPase contributes uniquely to *A. baumannii* growth, morphology, and overall fitness. These enzymes function in distinct, non-redundant pathways to support PG biosynthesis and homeostasis across different phases of the cell cycle.

RESULTS

Morphological defects associated with deletion of *dacC*, *dacD*, or *pbpG*

Given that *A. baumannii* encodes only three to four predicted DD-CPases, relative to at least seven in *E. coli* (29), we hypothesized that single-gene deletions in *A. baumannii* may result in distinct morphological phenotypes, offering fundamental insights into the specific roles of these enzymes.

Morphological defects were evident in each *A. baumannii* DD-CPase mutant (Fig. 1). The Δ*dacC* mutant exhibited a population of short, spherical cells relative to wild-type (WT) strain ATCC 17978 (Fig. 1A). Quantitative measurements confirmed a significant reduction in cell length and width (Fig. 1B; Fig. S1A). Complementation of PBP5/6a from a non-native locus rescued the cell morphology (Fig. 1A and B; Fig. S1A and B).

In contrast, the Δ*dacD* mutant displayed an elongated cell morphology with some heterogeneity (Fig. 1A and B; Fig. S1A), and increased D-amino acid modification of PG (Fig. 1C). Cells were stained with a fluorescent derivative of D-alanine (HADA) (34), which is incorporated into PG by PBPs and LD-TPases (35–38), and enables D-amino acid modification measurements. Increased modification with D-alanine may arise from increased tetrapeptide pools, which are substrates for the LD-TPase LdtJ (18), or from loss of PBP6b-mediated D-amino acid trimming from pentapeptides. While the precise mechanism remains unclear, these findings suggest a regulatory role for PBP6b in D-amino acid incorporation into position 5 of the peptide. Growth rate was similar to wild type (Fig. S1C), and complementation fully restored the wild-type morphology and fluorescence pattern (Fig. 1A through C; Fig. S1A).

To assess strain-specific effects, we analyzed DD-CPase mutants in a second *A. baumannii* background, the well-characterized clinical isolate AB5075 (39), using transposon mutants from the Manoil library (40). Similar shape and growth defects were observed in the AB5075 Δ*dacC* and Δ*dacD* mutants (Fig. S2), supporting the same effects for enzymatic inactivation across different strains, with the exception that the Δ*dacD* mutant did not show an elongated cell morphology in strain AB5075. Length, width, fluorescence intensity, and growth curve calculations were similar to trends described in strain ATCC 17978 (Fig. S2A through E).

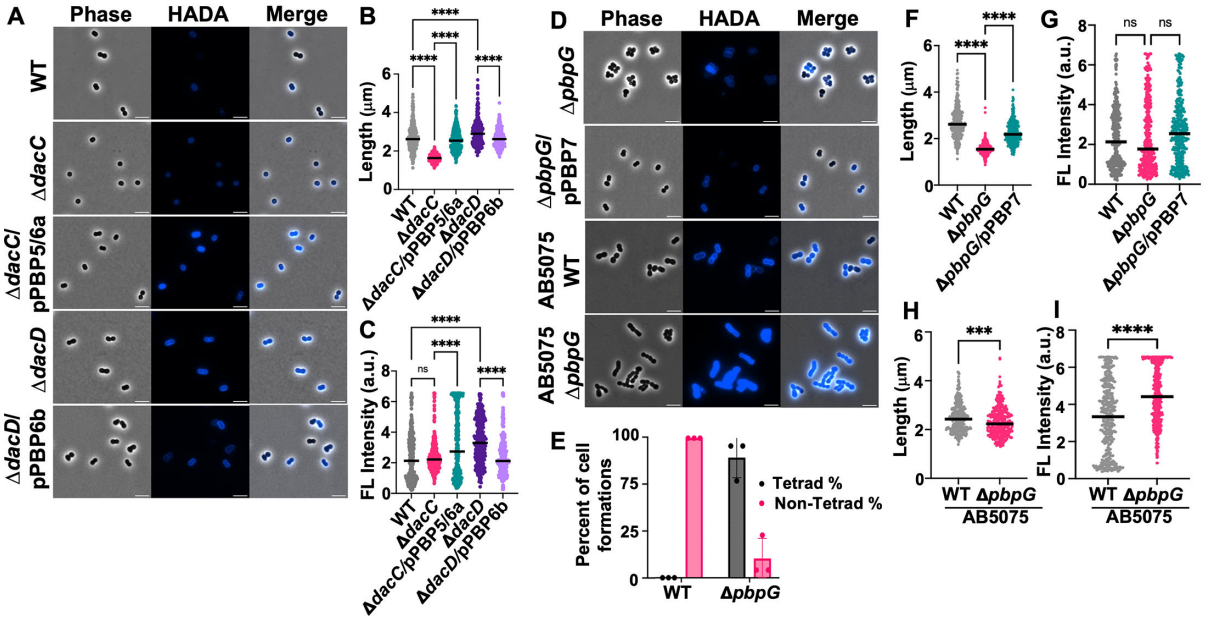

FIG 1 Microscopy of *A. baumannii* mutants in logarithmic growth phase. (A) Phase-contrast (left), fluorescence (middle), and merged (right) images of WT strain ATCC 17978, Δ*dacC*, Δ*dacC*/pPBP5/6a, Δ*dacD*, and Δ*dacD*/pPBP6b. Scale bar: 5 µm. (B) Quantification of cell length (pole to pole) for each cell population ($n \geq 300$), measured using ImageJ software with the MicrobeJ plugin. Each dot represents a single cell. Error bars indicate standard deviation. Statistical significance was determined using one-way ANOVA (***$P < 0.001$, ****$P < 0.0001$, ns = not significant). (C) Fluorescence intensity quantifications for Δ*dacC* and Δ*dacD*. a.u., arbitrary units. (D) Microscopy images, as described in panel A, showing strains ATCC 17978 Δ*pbpG*, Δ*pbpG*/pPBP7, AB5075 WT, and AB5075 Δ*pbpG*. (E) Quantification of coccobacilli and tetrad formations in strain ATCC 17978 WT and Δ*pbpG* using ImageJ software ($n \geq 300$). Tetrads are reported as a percentage of the total population. Data were collected from three independent experiments; one representative image and data set are shown. (F) Quantification of cell length for strain ATCC 17978 Δ*pbpG*, as described in panel B. (G) Fluorescence intensity quantifications for strain ATCC 17978 Δ*pbpG*. (H) Quantification of cell length for strain AB5075 WT and Δ*pbpG*, as described in panel B. (I) Fluorescence intensity quantifications for strain AB5075 WT *and* Δ*pbpG*.

Our previous work demonstrated that PBP7 (encoded by *pbpG*) exhibits DD-CPase and DD-EPase activity and is important for antibiotic survival (31). In strain ATCC 17978, Δ*pbpG* mutants formed spherical cells that clustered into tetrads, suggesting altered septum positioning and/or impaired cell separation (Fig. 1F and G). These cells also showed reduced length (Fig. 1H), width (Fig. S3A), and slightly decreased fluorescence upon treatment with HADA (Fig. 1I). Complementation restored wild-type morphology and growth (Fig. 1F, H, and I; Fig. S3A and B). This phenotype may reflect a combined lack of DD-CPase and DD-EPase activities.

In strain AB5075, Δ*pbpG* mutants also formed spherical cells but did not form tetrads (Fig. 1F). Instead, they formed chains of rounder cells (Fig. 1J and Fig. S3C), indicating a defect in cell elongation and separation. Cells also showed increased HADA fluorescence (Fig. 1K), suggesting increased PG D-amino acid modification and/or reduced removal. The strain-specific differences suggest that while PBP7 plays a consistent enzymatic role affecting morphology, additional functions may vary in different *A. baumannii* genetic backgrounds.

Morphological and growth defects associated with combined deletions of *dacC*, *dacD*, and *pbpG*

While single DD-CPase mutants in *A. baumannii* exhibit distinct morphological and growth phenotypes, previous studies in *E. coli* have shown that only multiple deletions (28), particularly in the Δ*dacA* background, are required to elicit significant morphological defects, suggesting functional redundancy among DD-CPases. To determine whether paired deletions in *A. baumannii* would exacerbate phenotypic defects, we engineered the Δ*dacC* Δ*dacD*, Δ*dacC* Δ*pbpG*, and Δ*dacD* Δ*pbpG* double mutants in strain ATCC 17978 (Fig. 2). Surprisingly, the double mutants did not exhibit exacerbated phenotypes.

Instead, each double mutant was characterized by a combination of the respective single-mutant characteristics. In the Δ*dacC* Δ*dacD* mutant (Fig. 2A), cells appeared spherical, like Δ*dacC* cells, but with increased morphological heterogeneity (Fig. 2B). Interestingly, the additional deletion of *dacD* rescued the slower growth observed in the Δ*dacC* single mutant (Fig. S3D). HADA incorporation was significantly higher relative to wild type (Fig. 2C), resembling the Δ*dacD* phenotype (Fig. 1C). These findings suggest that PBP5/6a and PBP6b have distinct functions: PBP5/6a in cell elongation, whereas PBP6b is involved in D-amino acid incorporation into PG. The increase in D-amino acid modification may compensate for the loss of PBP5/6a, thereby restoring normal growth.

In the Δ*dacC* Δ*pbpG* double mutants, the cells were spherical (Fig. 2A and B), consistent with elongation defects observed in both single mutants (Fig. 1A). However, the phenotype was not more severe, implying that PBP5/6a and PBP7 may have overlapping roles in cell elongation. HADA fluorescence intensity remained similar to wild type (Fig. 2C). Notably, tetrad cell clusters, indicative of altered septum positioning and/or cell separation defects, were formed (Fig. 2A), mirroring the Δ*pbpG* phenotype (Fig. 1F and K). A growth defect was also observed, and after 12 h, cell growth appeared compromised (Fig. S3D), suggesting a synthetic fitness defect in the double mutant.

The Δ*dacD* Δ*pbpG* mutant displayed short, spherical cells similar to the Δ*pbpG* single mutant cells (Fig. 2A and B). However, unlike in other Δ*pbpG* mutants in the ATCC 17978 background, these cells did not consistently form tetrads. While some tetrads were present, most cells existed as single short units or chains (Fig. 2D), indicating that Δ*dacD* disruption partially rescues the defect associated with *pbpG* deletion. This mutant also showed improved growth (Fig. S2D) and elevated HADA fluorescence intensity, consistent with increased D-amino acid incorporation or less removal (Fig. 2C). Together, these results suggest that *A. baumannii* DD-CPases have both distinct and overlapping roles in PG biosynthesis and remodeling and envelope homeostasis. The absence of additive morphological defects in DD-CPase double mutants highlights the complexity of their functions and suggests compensatory mechanisms that buffer against loss of individual enzymes.

Muropeptide analysis in the DD-CPase mutants reveals altered PG structures

To investigate how PBP5/6a and PBP6b contribute to *A. baumannii* PG structure, we analyzed the muropeptide compositions of the wild type and Δ*dacC,* and Δ*dacD* mutants in exponential and stationary phases (Fig. 3; Table S2), as previously done with the Δ*pbpG* mutant (31). PG was isolated and digested with a muramidase, and the resulting muropeptides were reduced with sodium borohydride and analyzed by high-performance liquid chromatography (HPLC), as previously described (18, 31, 41). Each mutant exhibited distinct muropeptide profiles relative to wild type. Wild-type strain ATCC 17978 showed the typical profile of a tetrapeptide-rich PG with only minor differences between growth phases (Fig. 3A and D). In contrast, Δ*dacC* mutants displayed the presence of more pentapeptide-containing muropeptides during both exponential and stationary phases (Fig. 3B and E), indicating that PBP5/6a is required for trimming D-alanine residues from pentapeptides—a hallmark of DD-CPase activity (16).

Δ*dacD* mutants also showed pentapeptide enrichment during exponential growth, consistent with DD-CPase activity. However, in both growth phases, these mutants exhibited elevated levels of D-amino acid-modified tetrapeptides (Fig. 3C and F). This increase correlates with the enhanced fluorescence observed in Δ*dacD* cells labeled HADA (Fig. 1A and C), suggesting that PBP6b may regulate D-amino acids incorporation into PG.

Peptides with D-amino acids (e.g., HADA) at position 4 and 5 are formed by exchange reactions with the terminal D-Ala on tetrapeptides and pentapeptides, respectively. PBPs exchange D-amino acids at position 5, resulting in tetrapeptide-D-amino acid (tetrapeptides with an additional amino acid at position 5), while LD-TPases exchange D-amino acids at position 4, resulting in tripeptide-D-amino acids. DD-CPases are only expected to remove D-amino acids from position 5. Hence, D-amino acid-modified tetrapeptides

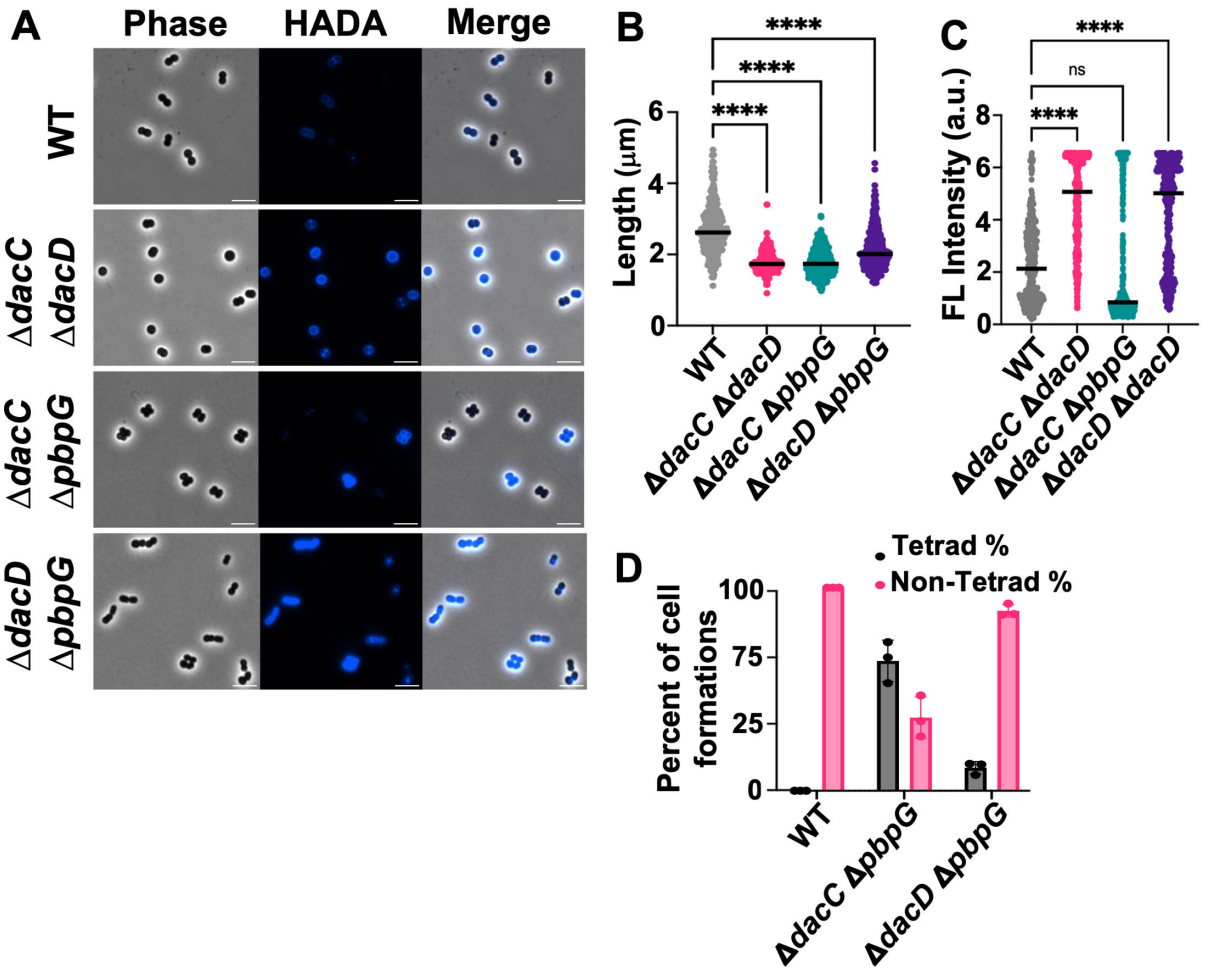

FIG 2 Microscopy of *A. baumannii* strain 17978 double mutants. (A) Phase-contrast (left), fluorescence (middle), and merged (right) images of WT, Δ*dacC* Δ*dacD*, Δ*dacC* Δ*pbpG*, and Δ*dacD* Δ*pbpG*. Scale bar: 5 µm. (B) Quantification of cell length (pole to pole) for each cell population ($n \geq 300$) was calculated using ImageJ software with the MicrobeJ plugin. Each dot represents one cell. Error bars represent standard deviation. Statistical significance was determined using one-way ANOVA (****$P < 0.0001$, ns = not significant). (C) Quantification of fluorescence intensity. (D) Quantification of coccobacilli and tetrad cell formations using ImageJ software ($n \geq 300$). Tetrads are reported as a percentage of the total population. Data were collected from three independent experiments; one representative image and data set are shown.

could be enriched due to loss of PBP6b-mediated trimming of D-amino acids from pentapeptides. Notably, pentapeptide enrichment was only observed during exponential growth, suggesting that PBP6b functions as a DD-CPase primarily during active cell wall synthesis while promoting D-amino acid removal during stationary phase.

Together, these results support distinct roles for PBP5/6a and PBP6b in PG remodeling: PBP5/6a primarily trims pentapeptides to tetrapeptides and regulates cell elongation, while PBP6b modulates D-amino acid incorporation, in the stationary phase, both potentially influencing PG cross-linking and envelope stability.

PBP5/6a and PBP6b are DD-CPases that catalyze tetrapeptide formation, and PBP6b is also an EPase

To validate the proposed enzymatic functions of PBP5/6a and PBP6b supported by PG analysis, we performed activity assays using the purified recombinant enzymes (Fig. S4). Native PBP5/6a and PBP6b, along with their respective catalytically inactive mutants (PBP5/6a$_{S121A}$ and PBP6b$_{S122A}$), in which the catalytic active serine was substituted with alanine, were expressed and purified. Each enzyme was incubated with muropeptides

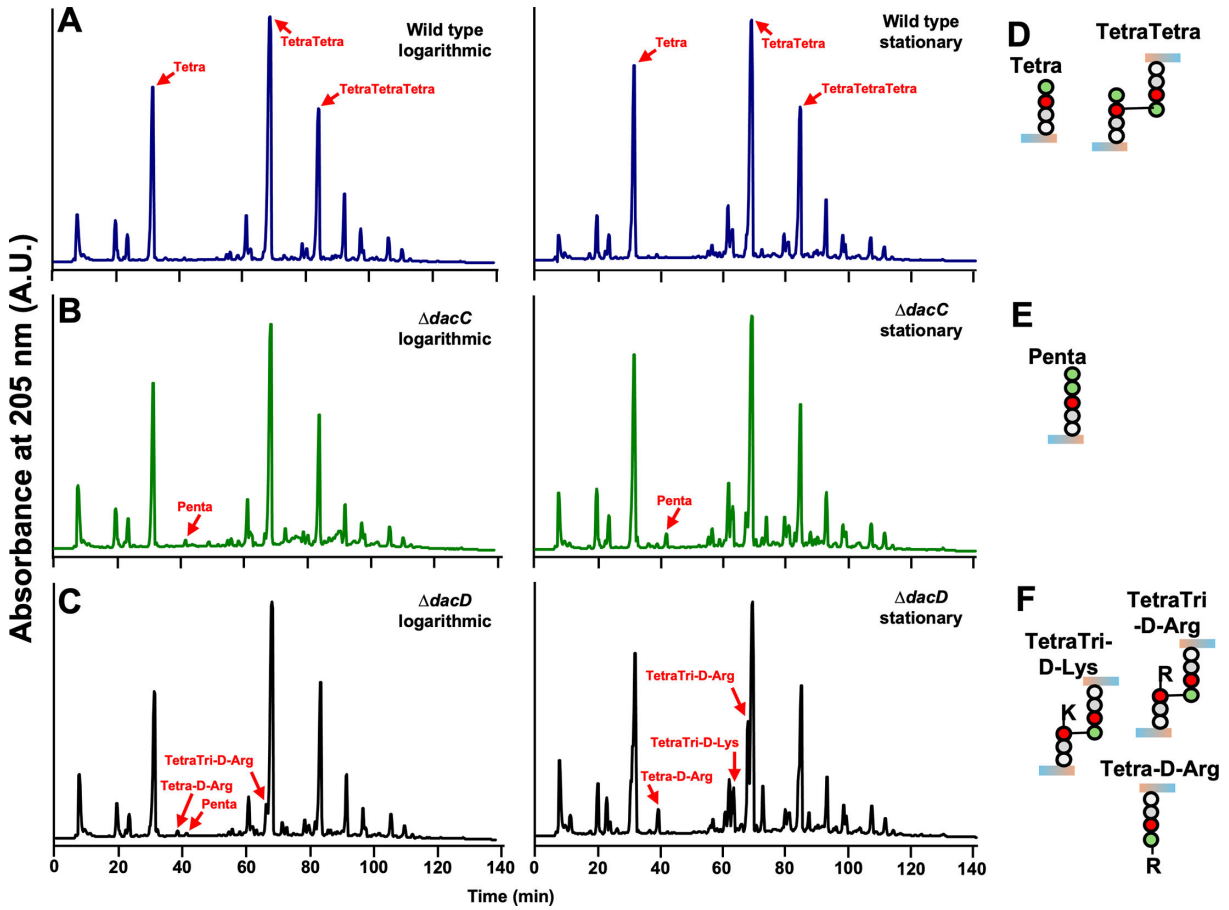

FIG 3 Muropeptide analysis in *A. baumannii* strain 17978 Δ*dacC* and Δ*dacD* mutants. Peptidoglycan was isolated from (A) wild-type, (B) Δ*dacC*, and (C) Δ*dacD* strains during logarithmic (left) or stationary (right) growth phases and analyzed by HPLC. The Δ*dacC* mutant exhibited enrichment of pentapeptides, while the Δ*dacD* mutant showed increased levels of D-modified muropeptides relative to wild type. Red arrows indicate peaks corresponding to specific muropeptide structures. (D, E, and F) Structural illustrations of the labeled muropeptides shown in panels A–C.

from *E. coli* CS703-1—enriched in pentapeptides—as previously described (31), and reactions were conducted at both pH 7.5 and pH 5.0 to assess pH-dependent activity.

PBP5/6a exhibited robust DD-CPase activity, as evidenced by a marked reduction in pentapeptide peaks and a corresponding increase in tetrapeptides at both pH values (Fig. 4A). No activity was observed in the reactions containing the PBP5/6a$_{S121A}$ active site mutant or in the no-enzyme controls. Additionally, PBP5/6a reduced TetraPenta levels while increasing TetraTetra muropeptides, further supporting its DD-CPase activity.

PBP6b was also active against pentapeptides and tetrapentapeptides, converting these to Tetra and TetraTetra muropeptides, respectively, at pH 7.5 (Fig. 4B). Interestingly, under acidic conditions at pH 5.0, more so than at pH 7.5, PBP6b showed robust DD-EPase activity. This dual activity was dependent on the catalytic serine residue, as the PBP6b$_{S122A}$ active site mutant and no-enzyme controls showed no such changes.

Together, these results confirm that PBP5/6a and PBP6b catalyze formation of tetrapeptides from pentapeptides, consistent with their role as DD-CPases, as anticipated by sequence homology and PG analysis. Moreover, PBP6b exhibits pH-dependent DD-EPase activity, potentially contributing to PG remodeling under acidic conditions, as previously observed for *E. coli* PBP6b, which only showed DD-CPase activity (29).

PBP5/6a and PBP7 play unique roles under pH stress

To determine whether *A. baumannii* DD-CPases contribute to environmental stress tolerance, we assessed the growth and cell morphology defects of Δ*dacC*, Δ*dacD*, Δ*pbpG*

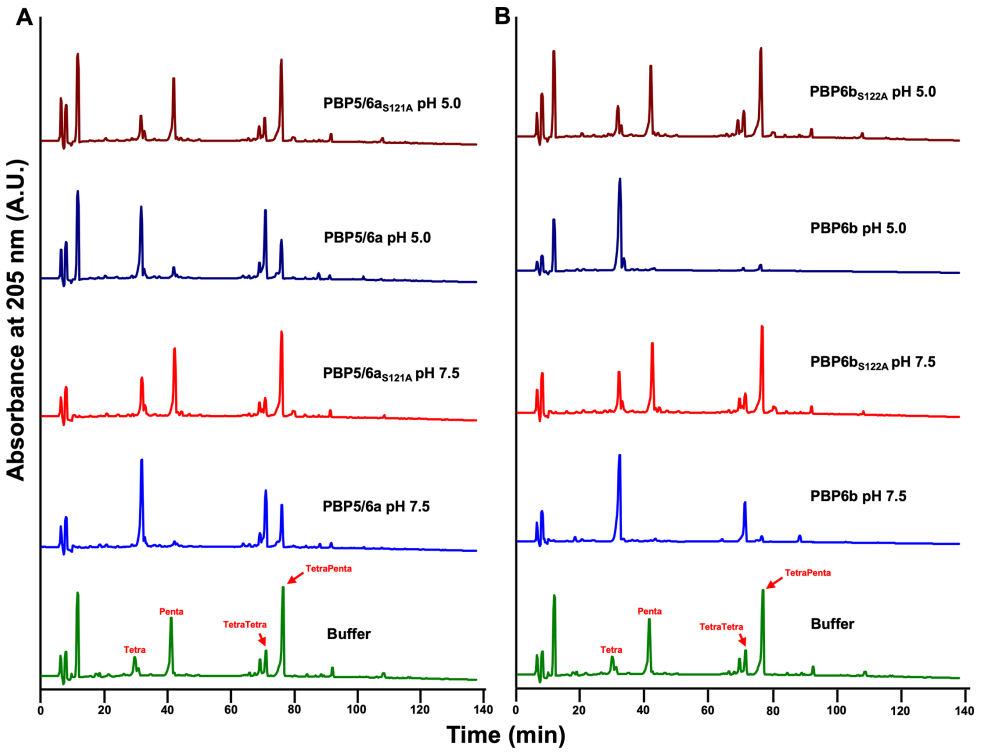

FIG 4 PBP5/6 and PBP6b exhibit DD-carboxypeptidase activity, and PBP6b also functions as an endopeptidase. (A) Recombinant PBP5/6 and its active site mutant PBP5/6$_{S121A}$, and (B) PBP6b and its active site mutant PBP6b$_{S122A}$, were incubated with peptidoglycan isolated from *E. coli* D456 (CS703-1), which contains Tetra, Penta, TetraTetra, and TetraPenta as the major components. Both PBP5/6 and PBP6b exhibited DD-carboxypeptidase activity, cleaving pentapeptides, whereas the active-site mutants showed no activity. PBP6b also demonstrated endopeptidase activity at both neutral (pH 7.5) and acidic pH (pH 5.0) conditions. Enzymes were used at a final concentration of 10 µM. Muropeptides are labeled in red.

mutants under acidic or alkaline conditions (Fig. 5). The Δ*dacC* mutant exhibited growth defects in acidic (pH 5.0) and alkaline conditions (pH 9.2), showing reduced growth in both relative to neutral pH (pH 7.5) (Fig. 5A). These findings suggest that PBP5/6a is required for maintaining cell envelope integrity across a broad pH range and that its function cannot be compensated by other DD-CPases.

In contrast, the Δ*dacD* mutant did not show obvious growth defects under any tested condition (Fig. 5A). Interestingly, this mutant displayed enhanced tolerance to alkaline and acidic pH relative to wild type, suggesting that PBP6b inactivation confers a selective advantage in stress environments, potentially by altering PG remodeling or D-amino acid incorporation (Fig. 3C and 4B).

The Δ*pbpG* mutant was highly sensitive to both acidic and alkaline conditions, with complete growth inhibition at pH 9.2 (Fig. 5A). This indicates that PBP7 is essential for survival under pH stress and, like PBP5/6a, its function is not redundant with other DD-CPases.

DD-carboxypeptidase mutants exhibit unique morphological responses under pH and osmotic stress

To further investigate the role of DD-CPases under environmental stress, we examined the morphology of Δ*dacC,* Δ*dacD*, and Δ*pbpG* cells using microscopy under acidic (Fig. 5B, D, and H, and Fig. S5A) or alkaline (Fig. 5C, F, G, and I, and Fig. S5B) conditions. In alkaline conditions, all strains—including wild type—exhibited enrichment of spherical cells (Fig. S5C, D, F, H, I, and K) and reduced HADA fluorescence intensity (Fig. S5E, G, and J) compared to neutral pH. These observations suggest that alkaline stress may affect cell

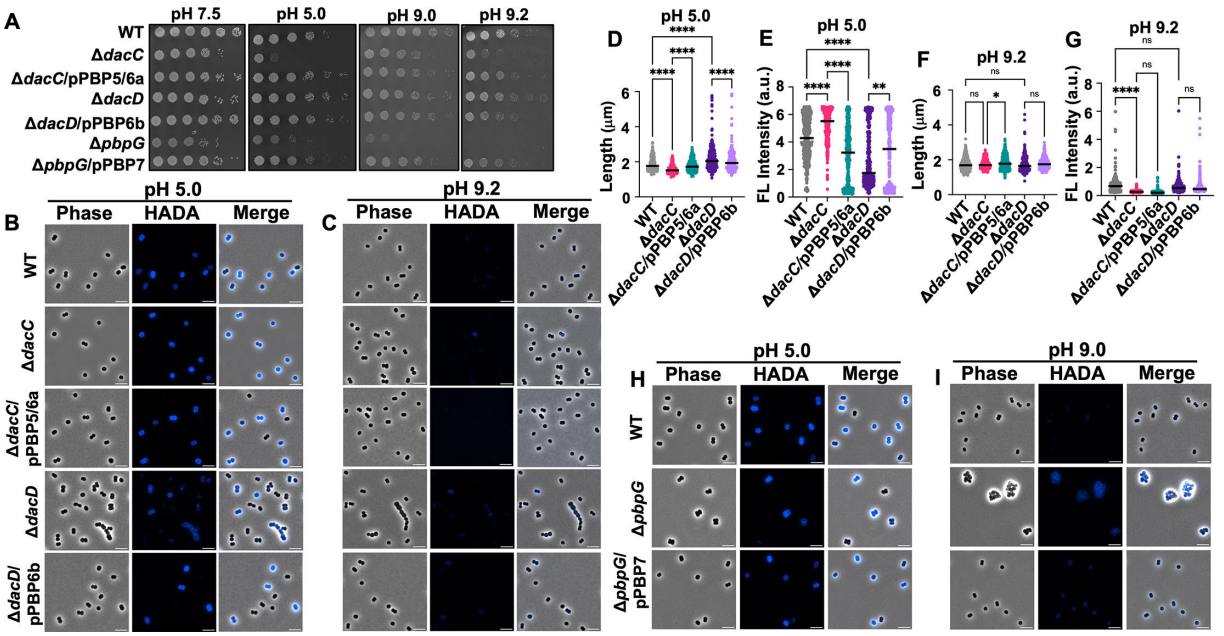

FIG 5 Colony growth and cell morphology of *A. baumannii* strain ATCC 17978 mutants under acidic and alkaline stress conditions. (A) Colony spot assays of WT and mutant strains serially diluted 10-fold starting at OD_{600} 0.05, plated on Luria-Bertani (LB) agar adjusted to the indicated pH values. (B) Phase-contrast (left), fluorescence (middle), and merged images of WT, Δ*dacC*, Δ*dacC*/pPBP5/6, Δ*dacD*, and Δ*dacD*/pPBP6b cells grown at pH 5.0. (C) Same as panel B, but cells grown at pH 9.2. Scale bar: 5 µm. (D) Quantification of cell length (pole to pole) at pH 5.0 of cell populations ($n \geq 300$), measured using ImageJ with the MicrobeJ plugin. Each dot represents a single cell. Error bars indicate standard deviation. Statistical significance was determined using one-way ANOVA (*$P < 0.05$, **$P < 0.01$, ****$P < 0.0001$, ns = not significant). (E) Quantification of fluorescence intensity at pH 5.0. (F) Same as panel D, but for cells grown at pH 9.0. (G) Same as panel E, but for cells grown at pH 9.0. (H) Phase-contrast (left), fluorescence (middle), and merged (right) images of WT, Δ*pbpG,* and Δ*pbpG*/pPBP7 cells grown at pH 5.0. (I) Same as panel H, but cells grown at pH 9.0. Each experiment was independently replicated three times, and one representative data set was reported.

elongation and D-amino acid modification of PG, likely through mechanisms independent of PBP5/6a and PBP6b. In contrast, acidic conditions led to shorter, brighter cells in the ATCC 17978 wild-type strain, consistent with reduced D-amino acid removal (Fig. S5E, G, and J). Mutants displayed similar length phenotypes at acidic pH relative to those observed at a neutral pH: Δ*dacC* cells were shorter, and Δ*dacD* cells were longer (Fig. 5D). However, a notable difference was the occasional appearance of chaining phenotypes in Δ*dacD* cells under both pH extremes (Fig. 5B through D), suggesting a potential role for PBP6b in cell separation during stress. HADA fluorescence intensity analysis revealed a striking shift at pH 5.0: Δ*dacC* cells showed increased fluorescence intensity relative to wild type, while Δ*dacD* cells showed reduced fluorescence (Fig. 5E). This suggests that PBP5/6a may remove incorporated D-amino acids under acidic conditions, a role previously attributed to PBP6b at neutral pH.

In the Δ*pbpG* mutants, tetrad-like cell clusters persisted under both acidic and alkaline conditions (Fig. 5H and I), but the nature of these clusters varied. Under acidic conditions, tetrads appeared as a single group of clustered cells, indicating a severe defect. In alkaline conditions, multiple tetrads aggregated into larger clusters, further compounding the phenotype. These morphological abnormalities likely contribute to the complete growth inhibition at pH 9.2 (Fig. 5A). The distinct responses under each stress condition suggest that PBP7 may have additional, condition-specific roles in regulating cell wall synthesis and envelope remodeling.

In addition to pH stress, we assessed whether DD-CPase mutants exhibit altered tolerance to osmotic stress. To test osmotic stress tolerance, we performed colony spot assays under hypo- and hyperosmotic conditions using LB agar with various NaCl concentrations (Fig. S6). Across all tested conditions, including Miller LB (171 mM NaCl), low-salt (0 mM NaCl), and high-salt environments (+250 mM NaCl), survival patterns were similar to wild type at under low salt conditions, except for Δ*pbpG*, which showed slightly

increased susceptibility at high salt. These findings suggest that PBP7 may contribute to adaptation under hypoosmotic stress.

DD-carboxypeptidases are not redundant in *Acinetobacter baumannii*

To further investigate the potential redundancy among DD-CPases, we performed complementation experiments by expressing other DD-CPases in single-mutant backgrounds (Fig. S7). In Δ*dacC* mutants complemented with pPBP6b or pPBP7, cells remained short and round, similar to the Δ*dacC* phenotype, indicating that neither enzyme restored elongation (Fig. S7A and B). Likewise, the Δ*dacD* mutant complemented with either pPBP5/6a or pPBP7 did not regain wild-type morphology. PBP5/6a expression produced a heterogeneous population of oblong and elongated cells, while PBP7 expression maintained elongated cells. Fluorescence intensity also remained high, confirming that *dacD* disruption could not be compensated for by other DD-CPases. In Δ*pbpG* mutants complemented with PBP5/6a and PBP6b, tetrad formation was eliminated, but the cells were still short and round, similar to the original Δ*pbpG* phenotype. These findings suggest that while other DD-CPases cannot compensate for elongation defects caused by *pbpG* loss, they may partially restore cell separation.

DISCUSSION

PG homeostasis—through coordinated synthesis, remodeling, and recycling—is essential for bacterial survival, morphology, and adaptation to environmental stress. Among the enzymes involved in PG remodeling and turnover, DD-CPases remain to be further studied in gram-negative bacteria other than *E. coli*. These enzymes trim terminal D-alanine residues from pentapeptides, generating tetrapeptides that influence PG cross-linking, cell shape, and stress resilience. In *E. coli*, DD-CPases are functionally redundant, with multiple enzymes compensating for one another depending on environmental conditions (29).

In this study, we characterized the roles of the putative DD-CPases PBP5/6a and PBP6b, and the DD-CPase/EPase PBP7 in *A. baumannii*, revealing different roles than their homologs in *E. coli*. Our results demonstrate that each DD-CPase in *A. baumannii* performs a unique, non-redundant function in PG homeostasis, cell shape maintenance, and environmental stress adaptation.

The Δ*dacC* mutant exhibited short spherical cells, implicating PBP5/6a in cell elongation. Δ*dacD* mutants, while slightly longer than wild type, displayed increased D-amino acid incorporation, suggesting that PBP6b may remove D-amino acids added by PBP-mediated exchange. Δ*pbpG* mutants exhibited the most severe defects, forming tetrad-like clusters, consistent with an important role for PBP7 in cell morphology and separation. These observed phenotypes were consistent also in the clinical isolate AB5075, although with some strain-specific morphological variation in the Δ*dacD* and, particularly, the Δ*pbpG* mutants.

Double mutant analysis further supported the non-redundant nature of these enzymes. Combinatorial deletions (Δ*dacC* Δ*dacD*, Δ*dacC* Δ*pbpG*, Δ*dacD* Δ*pbpG*) resulted in additive or compensatory phenotypes, but not in synthetic lethality. Notably, Δ*dacD* Δ*pbpG* mutants showed partial restoration of the Δ*pbpG* phenotype, suggesting that PBP6b may compensate for the morphological defects associated with PBP7 loss.

Muropeptide profiling revealed that Δ*dacC* mutants accumulated pentapeptides, confirming PBP5/6a's role in pentapeptide trimming. Δ*dacD* mutants showed enrichment of D-arginine- and D-lysine-acid-modified muropeptides, suggesting that PBP6b may specifically cleave these modified substrates or indirectly regulate their incorporation. These findings highlight the specialized substrate preferences and regulatory roles of individual DD-CPases in *A. baumannii*.

Enzymatic assays confirmed that both PBP5/6a and PBP6b possess DD-CPase activity. Additionally, PBP6b exhibited DD-EPase activity that increased at acidic pH, similar to the previously reported DD-EPase activity for PBP7 (31). This reduced specificity—combining

DD-CPase and DD-EPase activities—may explain the lack of redundancy among *A. baumannii* DD-CPases, in contrast to the environment-specific redundancy observed in *E. coli,* aside from PBP4's DD-CPase/EPase activity (29).

Environmental stress assays further emphasized the unique roles of these enzymes. Δ*dacC* and Δ*pbpG* mutants exhibited growth defects across all tested pH conditions, while Δ*dacD* mutants showed enhanced tolerance to alkaline stress. Morphological analysis under pH stress revealed that Δ*pbpG* mutants experienced exacerbated shape defects, with tetrads forming as single unseparated cells under acidic conditions and as aggregated clusters under alkaline conditions. These observations suggest that PBP7 may have additional, condition-specific roles in cell wall remodeling.

In conclusion, our study reveals that *A. baumannii* DD-peptidases are not functionally redundant but instead perform distinct, crucial roles in PG remodeling, cell shape maintenance, and stress adaptation. The multifunctionality of these enzymes—combining DD-CPase and DD-EPase activities—may reflect an evolutionary adaptation to optimize PG regulation in this clinically relevant pathogen. This streamlined adaptation could be advantageous for survival in hospital environments where this pathogen is frequently found and subjected to antibiotic pressures and desiccation. A simplified set of multifunctional enzymes could reduce metabolic burden and increase regulatory efficiency. *A. baumannii* presents a unique system of multifunctional DD-CPases. Only one other group of the ESKAPE pathogens presents consolidated DD-peptidases with the gram-positive *Staphylococcus aureus* containing one dual-activity DD-CPase/DD-EPase (PBP4) (7). Future studies should explore the broader regulatory networks and potential therapeutic vulnerabilities associated with these unique enzymes.

MATERIALS AND METHODS

Bacterial strains and growth conditions

Strains and plasmids used in this study are listed in Table S3. *Acinetobacter baumannii* strains were cultured aerobically from frozen stock on LB agar or in LB broth at 37°C. Unless otherwise specified, antibiotics were used at the following concentrations: 25 mg/L kanamycin and 10 mg/L tetracycline.

A. baumannii strain ATCC 17978 has been reported to consist of two distinct variants (42). To confirm the variant used in this study, colony PCR was performed using primers specific to the cardiolipin synthase gene (*clsC2*), which yielded a positive product, indicating that all experiments were conducted using the *A. baumannii* 17978 UN variant. *A. baumannii* strains, including AB5075, are known to exhibit phase-variable colony opacity phenotypes (43). Microscopic examination of AB5075 cultures revealed that most colonies were opaque, with only <1% translucent colonies observed among more than 200 colonies per plate (n = 3 plates per strain). For consistency, only opaque variants were used in all experiments, including those involving the AB5075 *dacA/C::tn*, *pbp6b::tn*, and *pbpG::tn* mutants.

Construction of genetic mutants

The primers used in this study are listed in Table S4 *A. baumannii* mutants, including Δ*dacC*, Δ*dacD*, Δ*pbpG*, and all double mutants, were generated using the recombination-mediated genetic engineering (recombineering), as previously described (18, 44–46). Briefly, a kanamycin resistance cassette flanked by FLP recombination target sites was PCR-amplified from the pKD4 plasmid using primers containing 125 bp homology arms specific to the target gene. The linear PCR product was electroporated into *A. baumannii* strain ATCC 17978, harboring the pRECAb plasmid (pAT03). Following recovery in LB broth, transformants were plated on LB agar supplemented with 7.5 mg/L kanamycin. All mutants were verified by PCR.

To remove the recombineering plasmid, mutants were grown on LB agar containing 2 mM nickel(II) chloride ($NiCl_2$) and replica-plated onto LB agar with either kanamycin

or tetracycline, as previously done (41). Colonies that were kanamycin-resistant and tetracycline-sensitive were confirmed by PCR to have lost the plasmid.

For markerless deletions, the kanamycin resistance cassette was excised by transforming the cured mutants with pMMB67EH::FLP (pAT08), which expresses FLP recombinase. Transformants were plated on LB agar containing tetracycline and 2 mM IPTG to induce recombinase expression. Successful excision of the resistance cassette was confirmed by PCR.

For complementation, the coding sequences of *dacC* (PBP5/6a), *dacD* (PBP6b), and *pbpG* (PBP7), including 200 bp of upstream and downstream flanking regions, were amplified from *A. baumannii* ATCC 17978 genomic DNA. These fragments were cloned into the pABBRknR plasmid at the XhoI and KpnI restriction sites. The resulting constructs (pPBP5/6a, pPBP6b, and pPBP7) were introduced into each single deletion mutant for analysis under the control of their native gene promoter.

Fluorescent HADA staining

Fluorescent D-Amino Acid staining was performed as previously described (18, 31, 47). Overnight cultures were grown with shaking at 37°C in 5 mL of LB broth, supplemented with appropriate antibiotics when necessary. The following day, cultures were diluted 1:100 into fresh LB medium (5 mL total volume) and incubated at 37°C with shaking until OD_{600} reached 0.3–0.5. The cells were harvested, washed to remove residual debris, and resuspended in 1 mL LB. Two microliters of 10 mM HCC-(linezolid-7-nitrobenz-2-oxa-1,3-diazol-4-yl)-amino-d-alanine (HADA) were added to each culture. The mixtures were incubated at 37°C for 20 minutes to allow incorporation of the fluorescent alanine. Following staining, cultures were washed with LB broth and fixed in phosphate-buffered saline (PBS) containing a 1:10 dilution of 16% paraformaldehyde.

Microscopy

Microscopy was performed as previously described (18, 31, 47). Paraformaldehyde-fixed cells were mounted on 1.5% agarose pads and imaged using an inverted Nikon Eclipse Ti-2 wide-field epifluorescence microscope. The system was equipped with a Photometrics Prime 95B camera and a Plan Apo 100× objective lens (NA 1.45). Phase-contrast and fluorescence images were acquired using NIS-Elements software. Blue fluorescence was visualized using a Sola LED light engine with the following filter set: 350/50 nm excitation filter, 460/50 nm emission filter, and a 400 nm dichroic mirror.

Image analysis

Microscopy images were processed as previously described (18, 31, 47). Pseudocoloring of fluorescence images was performed using ImageJ Fiji (48). Quantitative measurements, including length, width, fluorescence intensity, and total cell surface area, were measured using MicrobeJ (18, 31, 47, 49). Data were analyzed and visualized using GraphPad Prism version 10.2.2. Each experiment was independently repeated three times. Quantification data and images in the figures are from one representative biological replicate.

Peptidoglycan isolation

PG was isolated as previously described (18, 31, 41). Biological replicates were cultured in 400 mL of LB broth to either mid-logarithmic or stationary phase. Cells were harvested by centrifugation at 7,000 × *g* for 20 minutes at 4°C using an Avanti JXN-26 Beckman Coulter centrifuge with a JA-10 rotor. Pellets were resuspended in 6 mL of chilled PBS and lysed by dropwise addition of boiling 8% sodium dodecyl sulfate (SDS). PG was purified following the protocol established by Glauner et al. (50). Sacculi were treated with the Cellosyl muramidase (gift from Hoechst, Frankfurt am Main, Germany) to release muropeptides, which were then reduced with sodium borohydride and separated using

HPLC on a 250 × 4.6 mm, 3 µm Prontosil 120-3-C_{18} AQ reversed-phase column (Bischoff, Leonberg, Germany). Elution was monitored by absorbance at 205 nm. Muropeptide peaks were identified by comparison to published chromatograms (18, 41, 51).

Construction of PBP5/6a and PBP6b active-site mutants

To generate catalytically inactive variants of PBP5/6a and PBP6b, gene fragments encoding PBP5/6a$_{S121A}$ (serine 121 substituted with alanine) and PBP6b$_{S122A}$ (serine 122 substituted with alanine) were synthesized by Twist Biosciences. These mutations target the conserved serine residue in the active site, essential for enzymatic activity.

Construction of PBP5/6a and PBP6b overexpression strains

The coding sequences for *dacC* and *dacD* were amplified from *A. baumannii* ATCC 17978 genomic DNA, while *dacC*$_{S121A}$ and *dacD*$_{S122A}$ were amplified from synthesized gene fragment DNA. The amplicons were generated using primers that included a C-terminal His$_{8X}$-tag sequence to facilitate downstream purification. The resulting PCR products were cloned into the NdeI and BamHI restriction sites of the pT7-7Kn expression vector (52). The constructs pT7-7Kn::*dacC*, pT7-7Kn::*dacC*$_{S121A}$, pT7-7Kn::*dacD*, and pT7-7Kn::*dacD*$_{S122A}$ were transformed into *E. coli* C2987 chemically competent cells and confirmed by Sanger sequencing. Verified plasmids were subsequently transformed into *E. coli* C2527 (BL21) cells (New England BioLabs, Inc.) for protein expression and purification.

Purification of recombinant PBP5/6a and PBP6b

PBP expression and purification were done as previously described (31). Briefly, *E. coli* BL21 cells harboring pT7-7Kn::*dacC*, pT7-7Kn::*dacC*$_{S121A}$, and pT7-7Kn::*dacD*$_{S122A}$ were cultured in 1,000 mL of LB broth at 37°C until reaching OD_{600} 0.3–0.5. Due to toxicity associated with overexpression, 4,000 mL of culture was needed for *E. coli* BL21 cells harboring pT7-7Kn::*dacD*. 1L was sufficient with the other cultures. All cultures were induced with 1 mM IPTG for 4 hours at 25°C.

Following incubation, cells were harvested, washed with cold 1× PBS, and pelleted. Pellets were frozen overnight at −20°C, then thawed on ice and resuspended in 20 mL of lysis buffer (20 mM Tris, 300 mM NaCl, 10 mM imidazole, pH 8). Cells were lysed by sonication using a Fisher Scientific Model 120 Sonic Dismembrator, with 20 seconds on, followed by 20 seconds off, for a total of 10 cycles at 80% amplitude. Lysates were centrifuged at 15,428 × *g* for 10 minutes at 4°C. Pellets were resuspended in extraction buffer (25 mM Tris/HCl, 10 mM $MgCl_2$, 1 M NaCl, 0.02% NaN_3, 2% TX-100, pH 7.5) and incubated overnight at 4°C with gentle rocking. The next day, supernatants were collected by centrifugation and incubated with HisPur Ni-nitrilotriacetic acid resin (Thermo Scientific), pre-equilibrated with extraction buffer for 2 h at 4°C with rotation. The resin mixture was transferred to a 10-mL gravity-flow column and washed sequentially with 20 mL of lysis buffer containing increasing imidazole concentrations (0 mM, 15 mM, and 30 mM). Proteins were eluted in eight fractions using 500 µL of elution buffer (20 mM Tris, 300 mM NaCl, 250 mM imidazole, pH 8), incubated for 5 minutes before gravity elution. Fractions containing protein, identified by SDS-PAGE, were pooled and dialyzed overnight at 4°C in dialysis buffer (10 mM Tris, 50 mM KCl, 0.1 mM EDTA, 5% glycerol, pH 8) using 12 mL dialysis cassettes (Thermo Scientific). Protein purity and identity were confirmed by SDS-PAGE and bocillin-binding assays.

Activity assays

PBP5/6a and PBP6b activity assays were performed in a final reaction volume of 50 µL containing either neutral pH buffer (20 mM Tris/HCl, 50 mM NaCl, 2 mM $MgCl_2$ pH 7.5) or acidic pH buffer (20 mM sodium acetate, 50 mM NaCl, 2 mM $MgCl_2$, pH 5.0). Each reaction contained 10 µM of purified PBP5/6a, PBP5/6a$_{S121A}$, PBP6b, or PBP6b$_{S122A}$. PG isolated from *E. coli* CS703-1, enriched in pentapeptides, was added as a substrate.

Reactions were incubated at 37°C for 16 hours. Samples were boiled for 10 minutes to terminate reactions and incubated with 100 µg/mL cellosyl for a further 16 hours at 37°C. Samples were then boiled for 10 minutes and centrifuged at 16,000 × *g* for 10 minutes in a microfuge. The resulting muropeptides were reduced with sodium borohydride and acidified to a pH of 4.0–4.5. Control samples contained PG from *E. coli* CS703-1 without enzyme. Muropeptide analysis was performed as previously described (50).

Spot assays with pH medium

Overnight cultures were grown in LB broth at 37°C and then back-diluted to OD_{600} 0.05. Cultures were serially diluted 1:10 across five dilution steps. From each dilution, 5 µL aliquots were spotted onto LB agar plates adjusted to various pH levels. To prepare pH-adjusted LB plates, 50 mM Tris was added to standard LB agar, and the pH was adjusted to the desired value using either HCl or NaOH for the pH stress assays, while NaCl was adjusted to high (+250 mM NaCl) or low (0 mM NaCl). Plates were incubated at 37°C for 16 h, after which images were captured. All images shown are representative of three independent experiments.

Statistical analysis

Statistical analysis for cell morphology and fluorescence intensity data was performed using one-way ANOVA. A *P*-value of less than 0.05 was considered statistically significant.

ACKNOWLEDGMENTS

The work was supported by funding from the National Institutes of Health (grants R35GM143053 to J.M.B. and R01AI168159 to J.M.B. and W.V.) and the UK BBSRC (BB/W013630/1 to W.V.).

We thank Dr. Daniela Vollmer for the preparation of peptidoglycan.

AUTHOR AFFILIATIONS

[1]Department of Biological Sciences, University of Texas at Dallas, Richardson, Texas, USA
[2]Department of Cellular, Computational and Integrative Biology, (CIBIO), University of Trento, Trento, Italy
[3]Institute of Biophysics (IBF), National Research Council (CNR), FBK Nord, Trento, Italy
[4]Centre for Bacterial Cell Biology, Biosciences Institute, Newcastle University, Newcastle upon Tyne, United Kingdom
[5]Interdisciplinary Center for Medical Sciences (CISMed), University of Trento, Trento, Italy
[6]Institute for Molecular Bioscience, The University of Queensland, Brisbane, Queensland, Australia

AUTHOR ORCIDs

Arshya F. Tehrani http://orcid.org/0009-0001-8496-4944
Orietta Massidda https://orcid.org/0000-0001-8823-2372
Joseph M. Boll http://orcid.org/0000-0003-1412-9780

FUNDING

Funder	Grant(s)	Author(s)
National Institute of General Medical Sciences	R35GM143053	Joseph M. Boll
National Institute of Allergy and Infectious Diseases	R01AI168159	Joseph M. Boll

AUTHOR CONTRIBUTIONS

Arshya F. Tehrani, Conceptualization, Data curation, Formal analysis, Investigation, Methodology, Project administration, Resources, Software, Supervision, Validation,

Visualization, Writing – original draft, Writing – review and editing | Abhisha Khadka, Data curation, Formal analysis, Investigation | Berenice Furlan, Data curation, Formal analysis, Investigation, Methodology, Software, Validation, Visualization, Writing – review and editing | Michael Whalen, Conceptualization, Data curation, Formal analysis, Investigation, Methodology, Validation, Visualization, Writing – review and editing | Jacob Biboy, Data curation, Formal analysis, Investigation, Methodology, Resources, Writing – review and editing | Orietta Massidda, Conceptualization, Data curation, Formal analysis, Funding acquisition, Investigation, Methodology, Project administration, Resources, Software, Supervision, Validation, Visualization, Writing – review and editing | Waldemar Vollmer, Conceptualization, Data curation, Formal analysis, Funding acquisition, Investigation, Methodology, Project administration, Resources, Software, Supervision, Validation, Visualization, Writing – review and editing | Joseph M. Boll, Conceptualization, Data curation, Formal analysis, Funding acquisition, Investigation, Methodology, Project administration, Resources, Software, Supervision, Validation, Visualization, Writing – original draft, Writing – review and editing

ADDITIONAL FILES

The following material is available online.

Supplemental Material

Supplemental material (mBio00072-26-s0001.docx). Figures S1-S7; Tables S1-S4.

REFERENCES

1. Henderson JC, Zimmerman SM, Crofts AA, Boll JM, Kuhns LG, Herrera CM, Trent MS. 2016. The power of asymmetry: architecture and assembly of the gram-negative outer membrane lipid bilayer. Annu Rev Microbiol 70:255–278. https://doi.org/10.1146/annurev-micro-102215-095308
2. Vollmer W, Blanot D, de Pedro MA. 2008. Peptidoglycan structure and architecture. FEMS Microbiol Rev 32:149–167. https://doi.org/10.1111/j.1574-6976.2007.00094.x
3. Deghelt M, Cho S-H, Sun J, Govers SK, Janssens A, Dachsbeck AV, Remaut HK, Huang KC, Collet J-F. 2025. Peptidoglycan-outer membrane attachment generates periplasmic pressure to prevent lysis in gram-negative bacteria. Nat Microbiol 10:1963–1974. https://doi.org/10.1038/s41564-025-02058-9
4. Rojas ER, Billings G, Odermatt PD, Auer GK, Zhu L, Miguel A, Chang F, Weibel DB, Theriot JA, Huang KC. 2018. The outer membrane is an essential load-bearing element in gram-negative bacteria. Nature 559:617–621. https://doi.org/10.1038/s41586-018-0344-3
5. Fivenson EM, Rohs PDA, Vettiger A, Sardis MF, Torres G, Forchoh A, Bernhardt TG. 2023. A role for the gram-negative outer membrane in bacterial shape determination. Proc Natl Acad Sci USA 120:e2301987120. https://doi.org/10.1073/pnas.2301987120
6. Mamou G, Corona F, Cohen-Khait R, Housden NG, Yeung V, Sun D, Sridhar P, Pazos M, Knowles TJ, Kleanthous C, Vollmer W. 2022. Peptidoglycan maturation controls outer membrane protein assembly. Nature 606:953–959. https://doi.org/10.1038/s41586-022-04834-7
7. Sauvage E, Kerff F, Terrak M, Ayala JA, Charlier P. 2008. The penicillin-binding proteins: structure and role in peptidoglycan biosynthesis. FEMS Microbiol Rev 32:234–258. https://doi.org/10.1111/j.1574-6976.2008.00105.x
8. Goffin C, Ghuysen JM. 1998. Multimodular penicillin-binding proteins: an enigmatic family of orthologs and paralogs. Microbiol Mol Biol Rev 62:1079–1093. https://doi.org/10.1128/MMBR.62.4.1079-1093.1998
9. Nicola G, Peddi S, Stefanova M, Nicholas RA, Gutheil WG, Davies C. 2005. Crystal structure of *Escherichia coli* penicillin-binding protein 5 bound to a tripeptide boronic acid inhibitor: a role for Ser-110 in deacylation. Biochemistry 44:8207–8217. https://doi.org/10.1021/bi0473004
10. Denome SA, Elf PK, Henderson TA, Nelson DE, Young KD. 1999. *Escherichia coli* mutants lacking all possible combinations of eight penicillin binding proteins: viability, characteristics, and implications for peptidoglycan synthesis. J Bacteriol 181:3981–3993. https://doi.org/10.1128/JB.181.13.3981-3993.1999
11. Ghosh AS, Young KD. 2003. Sequences near the active site in chimeric penicillin binding proteins 5 and 6 affect uniform morphology of *Escherichia coli*. J Bacteriol 185:2178–2186. https://doi.org/10.1128/JB.185.7.2178-2186.2003
12. Dougherty TJ, Kennedy K, Kessler RE, Pucci MJ. 1996. Direct quantitation of the number of individual penicillin-binding proteins per cell in *Escherichia coli*. J Bacteriol 178:6110–6115. https://doi.org/10.1128/jb.178.21.6110-6115.1996
13. Ghosh AS, Melquist AL, Young KD. 2006. Loss of O-antigen increases cell shape abnormalities in penicillin-binding protein mutants of *Escherichia coli*. FEMS Microbiol Lett 263:252–257. https://doi.org/10.1111/j.1574-6968.2006.00429.x
14. Vollmer W, Joris B, Charlier P, Foster S. 2008. Bacterial peptidoglycan (murein) hydrolases. FEMS Microbiol Rev 32:259–286. https://doi.org/10.1111/j.1574-6976.2007.00099.x
15. Sieradzki K, Pinho MG, Tomasz A. 1999. Inactivated pbp4 in highly glycopeptide-resistant laboratory mutants of *Staphylococcus aureus*. J Biol Chem 274:18942–18946. https://doi.org/10.1074/jbc.274.27.18942
16. Höltje JV. 1998. Growth of the stress-bearing and shape-maintaining murein sacculus of *Escherichia coli*. Microbiol Mol Biol Rev 62:181–203. https://doi.org/10.1128/MMBR.62.1.181-203.1998
17. Glauner B, Höltje JV. 1990. Growth pattern of the murein sacculus of *Escherichia coli*. J Biol Chem 265:18988–18996. https://doi.org/10.1016/S0021-9258(17)30613-0
18. Kang KN, Kazi MI, Biboy J, Gray J, Bovermann H, Ausman J, Boutte CC, Vollmer W, Boll JM. 2021. Septal class A penicillin-binding protein activity and ld-transpeptidases mediate selection of colistin-resistant lipooligosaccharide-deficient *Acinetobacter baumannii*. mBio 12:e02185-20. https://doi.org/10.1128/mBio.02185-20
19. Nandy S, Tehrani AF, Hunt-Serracin AC, Biboy J, Pybus C, Vollmer W, Boll JM. 2025. Molecular interplay between peptidoglycan integrity and outer membrane asymmetry in maintaining cell envelope homeostasis. J Bacteriol 207:e00331-25. https://doi.org/10.1128/jb.00331-25
20. Typas A, Banzhaf M, Gross CA, Vollmer W. 2012. From the regulation of peptidoglycan synthesis to bacterial growth and morphology. Nat Rev Microbiol 10:123–136. https://doi.org/10.1038/nrmicro2677
21. Korat B, Mottl H, Keck W. 1991. Penicillin-binding protein 4 of *Escherichia coli*: molecular cloning of the dacB gene, controlled overexpression, and alterations in murein composition. Mol Microbiol 5:675–684. https://doi.org/10.1111/j.1365-2958.1991.tb00739.x

22. Vega D, Ayala JA. 2006. The DD-carboxypeptidase activity encoded by pbp4B is not essential for the cell growth of *Escherichia coli*. Arch Microbiol 185:23–27. https://doi.org/10.1007/s00203-005-0057-5
23. Broome-Smith JK, Ioannidis I, Edelman A, Spratt BG. 1988. Nucleotide sequences of the penicillin-binding protein 5 and 6 genes of *Escherichia coli*. Nucleic Acids Res 16:1617. https://doi.org/10.1093/nar/16.4.1617
24. Baquero MR, Bouzon M, Quintela JC, Ayala JA, Moreno F. 1996. dacD, an *Escherichia coli* gene encoding a novel penicillin-binding protein (PBP6b) with DD-carboxypeptidase activity. J Bacteriol 178:7106–7111. https://doi.org/10.1128/jb.178.24.7106-7111.1996
25. Henderson TA, Young KD, Denome SA, Elf PK. 1997. AmpC and AmpH, proteins related to the class C beta-lactamases, bind penicillin and contribute to the normal morphology of *Escherichia coli*. J Bacteriol 179:6112–6121. https://doi.org/10.1128/jb.179.19.6112-6121.1997
26. Egan AJF, Maya-Martinez R, Ayala I, Bougault CM, Banzhaf M, Breukink E, Vollmer W, Simorre J-P. 2018. Induced conformational changes activate the peptidoglycan synthase PBP1B. Mol Microbiol 110:335–356. https://doi.org/10.1111/mmi.14082
27. Spratt BG, Strominger JL. 1976. Identification of the major penicillin-binding proteins of *Escherichia coli* as D-alanine carboxypeptidase IA. J Bacteriol 127:660–663. https://doi.org/10.1128/jb.127.1.660-663.1976
28. Nelson DE, Young KD. 2000. Penicillin binding protein 5 affects cell diameter, contour, and morphology of *Escherichia coli*. J Bacteriol 182:1714–1721. https://doi.org/10.1128/JB.182.6.1714-1721.2000
29. Peters K, Kannan S, Rao VA, Biboy J, Vollmer D, Erickson SW, Lewis RJ, Young KD, Vollmer W. 2016. The redundancy of peptidoglycan carboxypeptidases ensures robust cell shape maintenance in *Escherichia coli*. mBio 7:e00819-16. https://doi.org/10.1128/mBio.00819-16
30. Morè N, Martorana AM, Biboy J, Otten C, Winkle M, Serrano CKG, Montón Silva A, Atkinson L, Yau H, Breukink E, den Blaauwen T, Vollmer W, Polissi A. 2019. Peptidoglycan remodeling enables *Escherichia coli* to survive severe outer membrane assembly defect. mBio 10:e02729-18. https://doi.org/10.1128/mBio.02729-18
31. Islam N, Kazi MI, Kang KN, Biboy J, Gray J, Ahmed F, Schargel RD, Boutte CC, Dörr T, Vollmer W, Boll JM. 2022. Peptidoglycan recycling promotes outer membrane integrity and carbapenem tolerance in *Acinetobacter baumannii*. mBio 13:e01001-22. https://doi.org/10.1128/mbio.01001-22
32. Romeis T, Höltje JV. 1994. Penicillin-binding protein 7/8 of *Escherichia coli* is a DD-endopeptidase. Eur J Biochem 224:597–604. https://doi.org/10.1111/j.1432-1033.1994.00597.x
33. Liu X, Boelter G, Vollmer W, Banzhaf M, den Blaauwen T. 2024. Peptidoglycan endopeptidase PBP7 facilitates the recruitment of FtsN to the divisome and promotes peptidoglycan synthesis in *Escherichia coli*. Mol Microbiol 122:743–756. https://doi.org/10.1111/mmi.15321
34. Kuru E, Hughes HV, Brown PJ, Hall E, Tekkam S, Cava F, de Pedro MA, Brun YV, VanNieuwenhze MS. 2012. *In situ* probing of newly synthesized peptidoglycan in live bacteria with fluorescent D - amino acids. Angew Chem Int Ed 51:12519–12523. https://doi.org/10.1002/anie.201206749
35. Kuru E, Lambert C, Rittichier J, Till R, Ducret A, Derouaux A, Gray J, Biboy J, Vollmer W, VanNieuwenhze M, Brun YV, Sockett RE. 2017. Fluorescent D-amino-acids reveal bi-cellular cell wall modifications important for *Bdellovibrio* bacteriovorus predation. Nat Microbiol 2:1648–1657. https://doi.org/10.1038/s41564-017-0029-y
36. Kuru E, Radkov A, Meng X, Egan A, Alvarez L, Dowson A, Booher G, Breukink E, Roper DI, Cava F, Vollmer W, Brun Y, VanNieuwenhze MS. 2019. Mechanisms of incorporation for d-amino acid probes that target peptidoglycan biosynthesis. ACS Chem Biol 14:2745–2756. https://doi.org/10.1021/acschembio.9b00664
37. Baranowski C, Welsh MA, Sham L-T, Eskandarian HA, Lim HC, Kieser KJ, Wagner JC, McKinney JD, Fantner GE, Ioerger TR, Walker S, Bernhardt TG, Rubin EJ, Rego EH. 2018. Maturing *Mycobacterium smegmatis* peptidoglycan requires non-canonical crosslinks to maintain shape. eLife 7:e37516. https://doi.org/10.7554/eLife.37516
38. García-Heredia A, Pohane AA, Melzer ES, Carr CR, Fiolek TJ, Rundell SR, Lim HC, Wagner JC, Morita YS, Swarts BM, Siegrist MS. 2018. Peptidoglycan precursor synthesis along the sidewall of pole-growing mycobacteria. eLife 7:e37243. https://doi.org/10.7554/eLife.37243
39. Jacobs AC, Thompson MG, Black CC, Kessler JL, Clark LP, McQueary CN, Gancz HY, Corey BW, Moon JK, Si Y, et al. 2014. AB5075, a highly virulent isolate of *Acinetobacter baumannii*, as a model strain for the evaluation of pathogenesis and antimicrobial treatments. mBio 5:e01076-14. https://doi.org/10.1128/mBio.01076-14
40. Gallagher LA, Ramage E, Weiss EJ, Radey M, Hayden HS, Held KG, Huse HK, Zurawski DV, Brittnacher MJ, Manoil C. 2015. Resources for genetic and genomic analysis of emerging pathogen *Acinetobacter baumannii*. J Bacteriol 197:2027–2035. https://doi.org/10.1128/JB.00131-15
41. Boll JM, Crofts AA, Peters K, Cattoir V, Vollmer W, Davies BW, Trent MS. 2016. A penicillin-binding protein inhibits selection of colistin-resistant, lipooligosaccharide-deficient *Acinetobacter baumannii*. Proc Natl Acad Sci USA 113:E6228–E6237. https://doi.org/10.1073/pnas.1611594113
42. Wijers CDM, Pham L, Menon S, Boyd KL, Noel HR, Skaar EP, Gaddy JA, Palmer LD, Noto MJ. 2021. Identification of two variants of *Acinetobacter baumannii* strain ATCC 17978 with distinct genotypes and phenotypes. Infect Immun 89:e00454-21. https://doi.org/10.1128/IAI.00454-21
43. Tipton KA, Dimitrova D, Rather PN. 2015. Phase-variable control of multiple phenotypes in *Acinetobacter baumannii* strain AB5075. J Bacteriol 197:2593–2599. https://doi.org/10.1128/JB.00188-15
44. Boll JM, Tucker AT, Klein DR, Beltran AM, Brodbelt JS, Davies BW, Trent MS. 2015. Reinforcing lipid A acylation on the cell surface of *Acinetobacter baumannii* promotes cationic antimicrobial peptide resistance and desiccation survival. mBio 6:e00478-15. https://doi.org/10.1128/mBio.00478-15
45. Tucker AT, Nowicki EM, Boll JM, Knauf GA, Burdis NC, Trent MS, Davies BW. 2014. Defining gene-phenotype relationships in *Acinetobacter baumannii* through one-step chromosomal gene inactivation. mBio 5:e01313-14. https://doi.org/10.1128/mBio.01313-14
46. Olea-Ozuna RJ, Campbell MJ, Quintanilla SY, Nandy S, Brodbelt JS, Boll JM. 2025. Alternative lipid synthesis in response to phosphate limitation promotes antibiotic tolerance in gram-negative ESKAPE pathogens. PLoS Pathog 21:e1012933. https://doi.org/10.1371/journal.ppat.1012933
47. Kang KN, Boll JM. 2022. PBP1A directly interacts with the divisome complex to promote septal peptidoglycan synthesis in *Acinetobacter baumannii*. J Bacteriol 204:e00239-22. https://doi.org/10.1128/jb.00239-22
48. Schindelin J, Arganda-Carreras I, Frise E, Kaynig V, Longair M, Pietzsch T, Preibisch S, Rueden C, Saalfeld S, Schmid B, Tinevez J-Y, White DJ, Hartenstein V, Eliceiri K, Tomancak P, Cardona A. 2012. Fiji: an open-source platform for biological-image analysis. Nat Methods 9:676–682. https://doi.org/10.1038/nmeth.2019
49. Ducret A, Quardokus EM, Brun YV. 2016. MicrobeJ, a tool for high throughput bacterial cell detection and quantitative analysis. Nat Microbiol 1:16077. https://doi.org/10.1038/nmicrobiol.2016.77
50. Glauner B, Höltje JV, Schwarz U. 1988. The composition of the murein of *Escherichia coli*. J Biol Chem 263:10088–10095. https://doi.org/10.1016/S0021-9258(19)81481-3
51. Le N-H, Peters K, Espaillat A, Sheldon JR, Gray J, Di Venanzio G, Lopez J, Djahanschiri B, Mueller EA, Hennon SW, Levin PA, Ebersberger I, Skaar EP, Cava F, Vollmer W, Feldman MF. 2020. Peptidoglycan editing provides immunity to *Acinetobacter baumannii* during bacterial warfare. Sci Adv 6:eabb5614. https://doi.org/10.1126/sciadv.abb5614
52. Boll JM, Hendrixson DR. 2011. A specificity determinant for phosphorylation in a response regulator prevents *in vivo* cross-talk and modification by acetyl phosphate. Proc Natl Acad Sci USA 108:20160–20165. https://doi.org/10.1073/pnas.1113013108